GA–A27409

VALIDATION STUDIES OF GYROFLUID AND GYROKINETIC PREDICTIONS OF TRANSPORT AND TURBULENCE STIFFNESS USING THE DIII-D TOKAMAK

by
C. HOLLAND, J.E. KINSEY, J.C. DeBOO, K.H. BURRELL, T.C. LUCE, C.C. PETTY, A.E. WHITE, T.L. RHODES, L. SCHMITZ, E.J. DOYLE, J.C. HILLESHEIM, G.R. McKEE, Z. YAN, S.P. SMITH, G. WANG, L. ZENG, B.A. GRIERSON, P. MANTICA, P.B. SNYDER, R.E. WALTZ, G.M. STAEBLER, and J. CANDY

OCTOBER 2012

GENERAL ATOMICS

DISCLAIMER

GA–A27409

VALIDATION STUDIES OF GYROFLUID AND GYROKINETIC PREDICTIONS OF TRANSPORT AND TURBULENCE STIFFNESS USING THE DIII-D TOKAMAK

by
C. HOLLAND,* J.E. KINSEY, J.C. DEBOO, K.H. BURRELL, T.C. LUCE, C.C. PETTY, A.E. WHITE,† T.L. RHODES,‡ L. SCHMITZ,‡ E.J. DOYLE,‡ J.C. HILLESHEIM,‡ G.R. McKEE,¶ Z. YAN,¶ S.P. SMITH, G. WANG,‡ L. ZENG,‡ B.A. GRIERSON,§ P. MANTICA,# P.B. SNYDER, R.E. WALTZ, G.M. STAEBLER, and J. CANDY

This is a preprint of a paper to be presented at the 24th IAEA Fusion Energy Conference, October 8–12, 2012, in San Diego, California and to be published in the *Proceedings.*

*University of California-San Diego, La Jolla, California.
†Massachusetts Institute of Technoloty, Cambridge, Massachusetts.
‡University of California-Los Angeles, Los Angeles, California.
¶University of Wisconsin-Madison, Madison, Wisconsin.
§Princeton Plasma Physics Laboratory, Princeton, New Jersey.
#Istituto di Fisica del Plasma "P. Caldirola," Associazione Euratom-ENEA-CNR, Milano, Italy.

Work supported by
the U.S. Department of Energy
under DE-FC02-04ER54698, DE-FG02-07ER54917,
DE-FG02-06ER54871, DE-FC02-99ER54512, DE-FG02-08ER54984,
DE-FG02-89ER53296, DE-FG02-08ER54999, DE-AC05-00OR22725,
and DE-AC02-05CH11231

GENERAL ATOMICS PROJECT 30200
OCTOBER 2012

Validation Studies of Gyrofluid and Gyrokinetic Predictions of Transport and Turbulence Stiffness Using the DIII-D Tokamak

C. Holland 1), J.E. Kinsey 2), J.C. DeBoo 2), K.H. Burrell 2), T.C. Luce 2), C.C. Petty 2), A.E. White 3), T.L. Rhodes 4), L. Schmitz 4), E.J. Doyle 4), J.C. Hillesheim 4), G.R. McKee 5), Z. Yan 5), S.P. Smith 2), G. Wang 4), L. Zeng 4), B. Grierson 6), P. Mantica 7), P.B. Snyder 2), R.E. Waltz 2), G.M. Staebler 2), and J. Candy 2)

[1] University of California-San Diego, La Jolla, California 92093, USA
[2] General Atomics, San Diego, California 92186-5608, USA
[3] Massachusetts Institute of Technology, Cambridge, Massachusetts 02139, USA
[4] University of California-Los Angeles, Los Angeles, California 90024, USA
[5] University of Wisconsin-Madison, Madison, Wisconsin 53706, USA
[6] Princeton Plasma Physics Laboratory, Princeton, New Jersey 08543-0451, USA
[7] Istituto di Fisica del Plasma "P. Caldirola," Associazione Euratom-ENEA-CNR, Milano, Italy

e-mail contact of main author: chholland@ucsd.edu

Abstract. A series of carefully designed validation experiments conducted on DIII-D to rigorously test gyrofluid and gyrokinetic predictions of transport and turbulence stiffness in both the ion and electron channels has provided an improved understanding of the experimental fidelity of those models over a range of plasma parameters. The first set of experiments conducted was designed to test predictions of H-mode core transport stiffness at fixed pedestal density and temperature. In low triangularity lower single null plasmas, a factor of 3 variation in neutral beam injection (NBI) heating was obtained, with modest changes to pedestal conditions that slowly increased with applied heating. The measurements and trends with increased NBI heating at both low and high injected torque are generally well-reproduced by the quasilinear TGLF transport model with the primary discrepancies arising from near-axis predictions of electron density and temperature profiles. Complementing these global stiffness studies, a second set of experiments was performed to quantify the relationship between the local electron heat flux Q_e and electron temperature gradient by varying the deposition profile of electron cyclotron heating (ECH) about a specified reference radius in low density, low current L-mode plasmas. Modeling of these experiments using both TGLF model and nonlinear gyrokinetic simulations with the GYRO code yields systematic underpredictions of the measured fluxes and fluctuation levels.

1. Introduction

An inherent feature of magnetic confinement based fusion energy (MFE) plasmas is the turbulent cross-field transport of particles, energy, and momentum, which generally determines the level of confinement achieved in the plasma, and thus the magnitude of fusion power generated [1]. This transport arises from a spectrum of nonlinearly coupled fluctuations with correlation lengths on the order of several ion gyroradii $\rho_i = V_{th,i}/\Omega_{ci}$ or smaller, which are generated by drift-wave instabilities driven by the inherent free energy gradients of the background equilibrium plasma. The magnitude of the turbulent fluxes generally dominates (neo)classical processes [2] away from the magnetic axis, and as such determines the relationship between the equilibrium profile dynamics and the external fueling, heating, and torque sources. Therefore, in order to confidently predict the performance of ITER and other next-step burning plasma devices, validated models of turbulent transport are required.

One of the defining characteristics of drift-wave turbulence is the sensitivity of the turbulent fluxes to the driving free energy gradients, often referred to as "transport stiffness." While there is no commonly accepted mathematical or formal definition of transport stiffness within the MFE community, the fundamental issue is that small changes in the equilibrium density, temperature, and rotation gradients can lead to large changes in the turbulent fluxes. In order to better appreciate the implications for realizing a viable MFE-based reactor, one

can invert this formulation to say that in a steady-state situation, a large increase in external heating (with a corresponding increase in the cross-field fluxes) may only lead to small increases in equilibrium gradients, and thus the stored energy and produced fusion power. Assessing the ability of transport models to accurately describe this stiffness is therefore essential for their validation.

Towards this end, a series of carefully designed validation experiments were conducted on DIII-D [3] to rigorously test gyrofluid and gyrokinetic predictions of transport and turbulence stiffness in both the ion and electron channels. In this paper, we present comparisons of transport predictions made using both the quasilinear gyrofluid transport model TGLF [4,5] and the nonlinear gyrokinetic code GYRO [6] to measurements from these experiments and corresponding power balance flux calculations (referred to as the experimental fluxes hereafter). For brevity, this paper focuses upon comparisons between model and simulation predictions against experiment, with limited discussion of the experimental results and details; more thorough discussions and characterizations of the experimental results can be found in Ref. 7. Motivated by modeling results previously reported at the 2010 IAEA FEC meeting, for which the predicted ITER fusion gain was highly sensitive to transport stiffness [8], in the first set of stiffness experiments we measured the response of core plasma profiles to increased neutral beam injection (NBI) heating at both low and high injected torque, while minimizing the changes in pedestal conditions. In Sec. 2, comparisons of core profiles predicted by the TGYRO transport solver [9] (using TGLF to predict turbulent fluxes) to measurements in these plasmas are presented. As a complement to these studies of "global" stiffness (i.e. the response of the core plasma as a whole to changes in injected heating and torque), a second set of experiments were conducted which varied the deposition profile of electron cyclotron heating (ECH) about a reference radius in low current, low density L-mode discharges to measure the relationship between local electron energy heat flux Q_e and normalized inverse electron temperature gradient scale length $a/L_{Te} = -d\ln T_e/d\rho$ (where ρ is the square root of the toroidal flux, normalized to a, its value at the separatrix). In Sec. 3, comparisons of both TGLF and GYRO predictions for the scaling of Q_e with a/L_{Te} against experiment are presented, as well as comparisons between experiment and GYRO predictions of $\delta T_e/T_{e0}$.

2. Transport stiffness validation studies in H-mode plasmas

In previously reported work [8], modeling of core confinement for the conventional 15 MA ELMing H-mode ITER scenario [10] using the quasilinear TGLF transport model predicted that the ITER core region (inside $\rho = 0.95$) would be very sensitive to the level of transport stiffness, in the sense that the fusion gain $Q = P_{fusion}/P_{aux}$ scaled as $Q \propto P_{aux}^{-0.8}$ *at fixed pedestal density and temperature*, with Q = 10 achieved at P_{aux} = 30 MW, $n_{e,ped} = 9 \times 10^{19}$ m^{-3}, and $T_{e,ped} = T_{i,ped} = 5$ keV. While TGLF has been shown to predict core profiles in DIII-D, JET, and TFTR discharges with a high degree of accuracy [5,8], these results motivated a new set of validation experiments focused on producing experimental conditions as similar as possible to the modeling—namely maintaining constant pedestal conditions as the auxiliary heating was increased. An additional motivation for the experiment arose from the observation that if one defines the local energy transport stiffness as $S = d\ln P_{tot}/d\ln z$, where P_{tot} is the total power flowing through a flux surface and $z = a/L_{Ti} + a/L_{Te}$ at that surface, then the level of stiffness in the ITER predictions is comparable to that seen in DIII-D and JET, as shown in Fig. 14 of Ref. 8.

To realize this goal of fixed pedestal conditions with increased heating, we utilized a lower single null configuration with low triangularity, which was previously found to have fixed pedestal $\beta = 2\mu_0 nT/B^2$ with varied input power [11]. Furthermore, in order to make

contact with both the ITER modeling (which assumed no equilibrium toroidal rotation or flow shear) as well as JET results [12] which found that local ion transport stiffness depended strongly upon rotation and magnetic shear, scans were done with both balanced and co-injected NBI heating. The experiments were run with $I_p = 1.2$ MA, $B_T = 2.16$ T, and line-averaged densities $\bar{n}_e$ between 3.1×10^{19} and 4.3×10^{19} m^{-3}. In these conditions, stable plasmas were obtained for 3.3, 5.4, and 7.2 MW of NBI heating at fixed injected torque of 1.4 – 1.6 N-m (the low torque scan), and at 3.3, 5.3, 7.1, and 9.2 MW of NBI heating with injected torque correspondingly rising from 2.9 to 6.4 N-m (the high torque scan). In each case, analysis windows 200 ms or greater were identified for which no core MHD activity was present. Representative profiles of n_e, T_e, T_i, and V_{tor} can be found in Fig. 1, and additional details of the experimental conditions and their analyses in Ref. 7. For the analysis presented here, a key finding was that while only modest changes were observed in the temperature profiles as the NBI injected power was scanned, there was a correspondingly clear increase in pedestal T_e and T_i values (for example, T_e increased from 0.6 to 0.8 keV and T_i from 0.8 to 1.1 at $\rho = 0.9$ in the low injected torque case). It is therefore important to emphasize that the assumption of fixed pedestal β with increasing injected power, which is an essential element of the motivating prediction of $Q \propto P_{aux}^{-0.8}$, may not be an experimentally realizable condition, and must be taken into account when projecting those results to actual ITER performance predictions. Despite this limitation, the obtained datasets provide a clear test for core transport models that can be used to assess our ability to accurately model core transport stiffness in H-mode conditions.

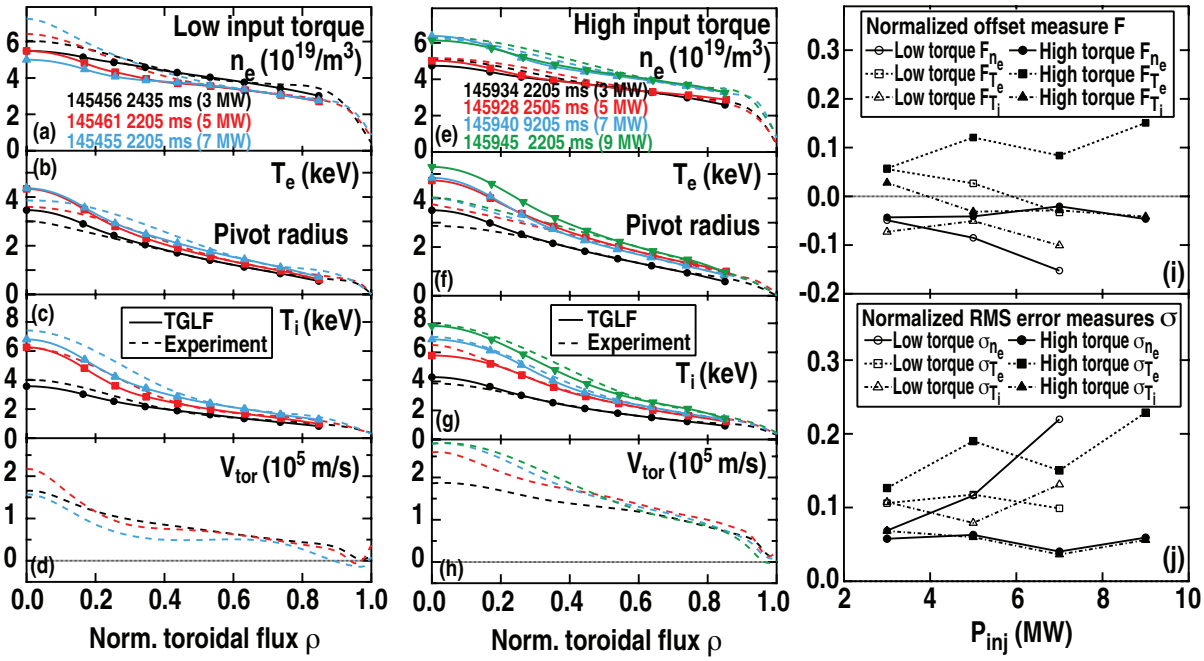

FIG. 1. Measured (a,e) n_e, (b,f) T_e, (c,g) T_i, and (d,h) V_{tor} profiles (- - -) for (a-d) low and (e-h) high injected beam torque. TGYRO-TGLF transport solution profiles (with pivot radiues at ρ=0.64) are plotted as solid curves with symbols denoting radial locations of each TGLF instance used in the prediction. A different symbol is used for each injected power level: 3 MW (●), 5 MW (■), 7 MW(▲), and 9 MW(▼). ITPA-defined metrics for (i) normalized offset F (Eq. 2) and (j) normalized error σ (Eq. 3) between transport solution and experimental profile fits, as a function of applied NBI heating power, for n_e (●), T_e (■), and T_i (▲). Open symbols denote the low torque cases, and closed symbols the high torque cases.

2.1. Comparison of TGLF transport solution profiles to experiment

In order to test the fidelity of the TGLF model in accurately predicting the measured core responses to increased NBI heating, so-called "transport solution" profiles have been calculated using the TGYRO transport solver. Transport solution profiles denote those profiles which, when input to a given transport model (or set of models) such as TGLF, yield predicted turbulent fluxes that satisfy the steady-state transport equations. In other words, the transport solutions $\left\{n^{TS}, T_e^{TS}, T_t^{TS}\right\}$ satisfy

$$\frac{1}{V'}\frac{\partial}{\partial r}\left\{V'\left(Q_{turb}\left(n^{TS}, T_i^{TS}, T_e^{TS}\right) + Q_{neo}\left(n^{TS}, T_i^{TS}, T_e^{TS}\right)\right)\right\} = S_{exch}(n^{TS}, T_i^{TS}, T_e^{TS}) + S_{aux} \quad . \tag{1}$$

Here, Q_{turb} denotes the turbulent flux, Q_{neo} the neoclassical flux, S_{exch} the exchange source term (which can include both classical and turbulent components [13]), and S_{aux} the externally applied auxiliary heating source; a third term representing self-heating due to fusion reactions can also be added to the right hand side if appropriate. It should be emphasized that the transport solution profiles simultaneously satisfy both the particle and energy balance equations for the specified external sources S_{aux}. TGYRO uses a novel nonlinear root-finding approach to solve Eq. 1, in which it efficiently solves for the radial profiles of $\vec{z} = \left\{a/L_{ne}, a/L_{Te}, a/L_{Ti}\right\}$ at a relatively modest number (generally on the order of 5-10) radial locations, with $\vec{z}(\rho = 0) = 0$ and taken to be piecewise linear between the radial instances. When combined with a specified pivot radius ρ* (which need not be the outermost radial instance) at which density and temperature values are held fixed, the piecewise-linear inverse scale length profiles $\vec{z}$ can be integrated to yield smoothly varying density and temperature profiles across the domain. In the work presented here, the toroidal rotation profiles are held fixed; implementation of self-consistently evolved rotation profiles in TGYRO which will satisfy momentum balance is currently underway and results using the capability will be presented in future work. The neoclassical contributions are calculated using the analytic Hinton-Hazeltine model [2] and are found to only be significant for ion transport at $\rho < 0.2$; tests using the NEO code [14] to directly solve the drift-kinetic equation yield no significant differences in predicted results.

For each condition obtained in the experimental scans, transport solution profiles have been calculated using 8 radial instances uniformly distributed over $0.14 \le \rho \le 0.84$. The TGYRO-TGLF transport solution profiles are plotted in Fig. 1 as solid curves, with solid symbols (varying with NBI power) denoting the locations of the radial instances. Examination of the profile data indicated that the rapid ELMs present in these discharges yielded clear perturbations into ρ = 0.7, which lead to the selection of the pivot radius ρ* = 0.64. While there are some discrepancies near the magnetic axis, the transport solutions generally capture the key observed features, particularly at $\rho > 0.35$ (although this may to some extent reflect the choice of ρ* = 0.64 as the pivot radius). In particular, the ion temperature profiles are quite well reproduced, include features such the increase in core T_i peaking in the 5.4 and 7.2 MW low torque cases relative to the 3.3 MW case. The primary discrepancies between the predictions and experiment arise from an underprediction of on-axis density in the low torque discharges, and overprediction of T_e inside ρ = 0.3-0.4, particularly in the high torque discharges. In order to quantify the fidelity of these predictions, the ITER Profile Database [15] metrics for the offset F and root-mean-square (RMS) error σ have been calculated as (averaging over $0 \le \rho \le 0.84$)

$$F = \frac{1}{N}\sum_j \varepsilon_j \Big/ \sqrt{\frac{1}{N}\sum_j T_{x,j}^2} \quad , \tag{2}$$

$$\sigma = \sqrt{\frac{1}{N}\sum_j \varepsilon_j^2} \Big/ \sqrt{\frac{1}{N}\sum_j T_{x,j}^2} \quad . \tag{3}$$

Here, $\varepsilon_j = T_s(\rho_j) - T_x(\rho_j)$ is the difference between the jth radial point of the transport solution profile T_s and experimental profile fit T_x. The results are plotted in Fig. 1(i) and 1(j), and show that except for a few cases, the offsets F have magnitudes < 10%, and RMS error σ are < 20%. The metrics quantify the key points outlined above that the electron temperature profiles are not as well predicted as the ion temperature profiles (particularly in the high injected torque case), although they do not reveal (as the profiles plots themselves do) that most of the discrepancy comes from small rather than large radii. In this vein, it is also worth noting that consistent with previous H-mode validation studies [16], we find no evidence of a systematic near-edge transport shortfall as is often seen for L-mode discharges [17-20].

The results presented here represent only the first step in the full range of planned validation studies using these experimental datasets. First, it should be emphasized that the metrics in Eqs. 2 and 3 were designed to test profile predictions made using the outermost radius modeled as the pivot point, and new metrics (based perhaps on gradients or scale lengths) are needed for better evaluations of profile predictions using interior pivot points (such as those presented here). Such metrics are currently under development, and their formulation and application will be presented in future work. The results presented here will also be extended to examine the effects of self-consistently evolving the rotation profiles to simultaneously satisfy momentum balance in addition to particle and energy balance, as well as investigating whether inclusion of turbulent energy exchanges significantly impacts these findings. In addition, more fundamental nonlinear gyrokinetic modeling of the transport and turbulence levels (measured via beam emission spectroscopy (BES) [21]) using the GYRO code has begun and will be reported in future work. Initial simulation results indicate that both the low and high torque cases lie in a regime in which strong low-k ($k_\theta \rho_s < 1$) ITG turbulence is almost completely suppressed by the equilibrium shear levels, with small changes to the input temperature and rotation gradients yielding results ranging from complete suppression of the low-k modes (and no meaningful ion energy or momentum transport) to significant low-k activity and transport several times larger than the power balance results.

3. Testing model predictions of local electron heat flux stiffness in L-mode plasmas

As a complement to the studies of global core profile stiffness discussed in Sec. 2, a second set of validation experiments was performed to obtain direct measurements of the local electron thermal transport and turbulence stiffness. In contrast to the H-mode experiments described in Sec. 2, these experiments were performed in low current (I_P = 0.8 MA), low density ($\bar{n}_e = 1.9 \times 10^{19}$ m^{-3}) L-mode discharges. In these experiments, the resonant location of five ECH gyrotron sources (each providing ~ 500 kW of heating) was systematically varied about a reference radius, starting from all sources resonant outside the reference surface to one source resonant inside and four outside configuration, and so on until all five were resonant inside the reference radius. Using this approach, a very fine scan in the electron energy flux Q_e flowing through the surface, and corresponding local changes in a/L_{Te}, were obtained, while maintaining the local absolute temperature and density values relatively constant, as well as the net heating power and edge boundary conditions. In addition to the manipulations in resonant location of these five sources, a sixth gyrotron source was kept resonant outside the reference radius, but modulated at 28 Hz in order to obtain heat pulse measurements of the transport. This procedure was performed in Ohmic plasmas with no other heating, as well as in plasmas in co, counter-, and balanced NBI

heating, about both $\rho = 0.4$ and 0.6 reference radii. In this paper we focus upon comparisons of model predictions to experimental results obtained for the conditions with only ECH heating centered about the $\rho = 0.6$ reference radius to experimental observations; additional experimental details for various heating cases can be found in Ref. 7 and 22.

The global response of the T_e profiles to the variations in ECH deposition profile are shown in Fig. 2(a), where the (x,y) labeling convention denotes the number of gyrotron sources resonant inside $\rho = 0.6$ (x) and the number outside (y), including the modulated source. A clear rise in T_e at and inside the reference radius is observed, while T_e remains constant beyond the reference radius. Fig. 2(b) plots Q_e at $\rho = 0.6$ as a function of the measured value of a/L_{Te}, the most notable feature of which is the sharp break in slope between the points with $a/L_{Te} = 2.2$ and 3. This change is also observed in the amplitude of local T_e fluctuations measured with correlation electron cyclotron emission (CECE) radiometry [18,23], as shown in Fig. 2(c). While such a break seems consistent in some ways with a critical gradient for the electron temperature, the fact that neither the fluxes nor fluctuation levels go to zero below this break requires a more nuanced discussion than is feasible here. As such, we only describe this feature as the break point in the flux and fluctuation scalings presented in this analysis.

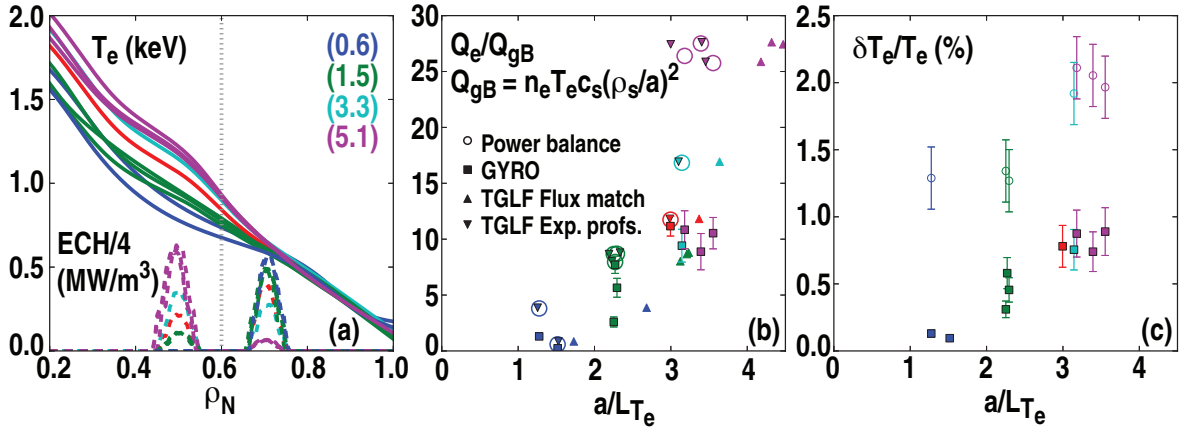

FIG. 2. (a) Response of T_e to changes in ECH deposition profile, (b) comparisons of TGLF and GYRO predictions of electron heat flux scaling with a/L_{Te} to experiment, and (c) comparisons of GYRO predictions of $\delta T_e/T_{e0}$ scaling with a/L_{Te} to experiment. Power balance calculations and experimental measurements are shown as (○), GYRO predictions as (■), TGLF predictions using the experimental profile fits as inputs as (▼), and local flux-matching TGLF predictions as (▲).

These observations have been used to test the ability of both TGLF and nonlinear global GYRO simulations to accurately identify the break point and predict the scaling of transport (and turbulence in the case of GYRO) levels about this point. Global GYRO simulations are used based upon findings of a recently published study examining similar DIII-D plasmas [20], which found that at low gradient levels local simulations resulted in unphysical streamer-type eddies with radial correlation lengths on the order of the radial domain size, while inclusion of nonlocal effects yielded turbulence with physically relevant radial correlation lengths; similar results were found in initial local simulations of these plasmas. The GYRO simulations included kinetic electrons (both passing and trapped), collisional effects, shaped geometry using a generalized Miller model [24], two gyrokinetic ion species (deuterium and carbon), and drift-kinetic electrons with fully realistic mass ratio $\sqrt{M_D/m_e} = 60$. The simulations are electrostatic based on the low values of β_e and linear studies which found no significant effect from their inclusion. The simulations used 40 toroidal modes with $\Delta n = 8$, corresponding to $0 \le k_y \rho_s \le 2.9$ with resolution

$\Delta\left(k_y\rho_s\right) = \Delta nq\rho_s/r_{\min} = 0.074$, and binormal domain size $L_y = 1/\Delta k_y = 85\rho_s$. The total radial domain spanned the range $0.5 < \rho < 0.7$, corresponding to 104 ρ_s; 300 radial grid points were used yielding a radial resolution of $\Delta r/\rho_s = 0.35$. Quasilinear relaxation of the equilibrium profiles was prevented by using buffer regions and damping of the longest radial wavelength components of the $n = 0$ fluctuations as described in Ref. 25. Integration was done using Runge-Kutta integration with timestep h=0.01 a/c_s, with the collisionless linear electron dynamics treated implicitly.

The first test of TGLF and GYRO was to simply input the local profile and gradient values derived from the experimental profile fits as inputs to the codes, and to then directly predict the local values of the particle and energy fluxes. Both codes predict values of Q_e consistent in both magnitude and scaling with a/L_{Te} at the lower experimental values below the break point, as shown in Fig. 2(b). However, only TGLF appears to reproduce the highest fluxes, while the GYRO predictions appear to saturate at values lower than those observed for the highest values. Moreover, both TGLF and GYRO predict very low levels of the ion heat flux Q_i (which arises from the collisional exchange term as $T_e > T_i$ in these plasmas), several times lower than the power balance calculations. TGLF also predicts non-negligible particle fluxes Γ_e for some cases, such that the convective electron energy flux $Q_e^{conv} = (3/2)T_e\Gamma_e$ can be up to 50% of the total Q_e plotted in Fig. 2(b). To account for these discrepancies, a second set of TGLF predictions were made, in which the local values of a/L_{Te}, a/L_{Ti}, and a/L_{ne} were systematically varied until the TGLF predictions of Q_i, Q_i, and Γ_e matched the local power balance calculations, while holding the local values of T_e, T_i, and n_e fixed. These results are also shown in Fig. 2(b), and demonstrate that the local flux-matching values of a/L_{Te} are systematically higher than those derived from the experimental fits. Along with this increase in a/L_{Te} relative to experimental values, we find that the local values of a/L_{Ti} must also be increased by 50% on average over the cases considered to match the local Q_i values, while a/L_{ne} must be reduced by 25% to yield no net particle flux (as the wall recycling source is assumed negligible at this radius). Developing a better understanding the full physics underlying this upshift in flux-matching a/L_{Te} values relative to the experimental measurements (e.g. in terms of a change in the balance of TEM to ITG modes, or the balance between ∇T_e and ∇n_e driven TEM modes) is ongoing and will be reported in future work. Work is also currently underway to implement the capability to calculate self-consistent flux-matching global GYRO simulations within the TGYRO code, with the aim of investigating cases such as these.

In Fig. 2(c), the GYRO predictions for the measured $\delta T_e/T_{e0}$ levels are shown, in which the measurements are estimated using a simple synthetic diagnostic proxy of 0.5 ± 0.1 times the RMS amplitude of the finite-n T_e fluctuations in the simulation. This range was chosen based on the findings of a variety of previous validation studies [18-20,25] which find the full synthetic diagnostic calculations which convolve the predicted fluctuations in the (R,Z) plane with a two-dimensional spatial transfer function all yield attenuation levels of the gyrokinetic $\delta T_e/T_{e0}$ predictions by 40%-60%. Interestingly, these predicted fluctuation levels are systematically lower than the observed levels by a factor of two or more, and there is no clear evidence for a break point in the predicted fluctuation levels as is seen experimentally. This finding is contrary to what was found in previous GYRO simulations of similar low density plasmas with only ECH heating [25], which predicted both Q_e values and $\delta T_e/T_{e0}$ levels consistent with power balance and measurement, even while underpredicting Q_i as is found here. Fully quantifying the sensitivity of these findings to uncertainties in the driving gradients is currently underway, and future work will report those results along with the impact of including the full synthetic CECE diagnostic algorithm in the fluctuation amplitude predictions.

Acknowledgments

This work was supported by the U.S. Department of Energy under DE-FG02-07ER54917, DE-FG02-06ER54871, DE-FC02-04ER54698, DE-FC02-99ER54512, DE-FG02-08ER54984, DE-FG02-89ER53296 and DE-FG02-08ER54999. The numerical simulations were performed as part of the research program of the Center for the Simulation of Plasma Microturbulence. This research used resources at the National Center for Computational Sciences at Oak Ridge National Laboratory, which is supported by the Office of Science of the Department of Energy under Contract DE-AC05-00OR22725. Additional simulations were performed which used resources of the National Energy Research Scientific Computing Center, which is supported by the Office of Science of the U.S. Department of Energy under Contract No. DE-AC02-05CH11231.

References

[1] HORTON, W., Rev. Mod. Phys. **71** (1999) 735.
[2] HINTON, F.L., *et al.*, Rev. Mod. Phys. **48** (1976) 239.
[3] LUXON, J.L., Nucl. Fusion **42** (2002) 614.
[4] STAEBLER, G.M., KINSEY, J.E., and WALTZ, R.E., Phys. Plasmas **14** (2007) 055909.
[5] KINSEY, J.E., STAEBLER, G.M., and WALTZ, R.E., Phys. Plasmas **15** (2008) 055908.
[6] CANDY, J. and WALTZ, R.E., J. Comput. Phys. **186** (2003) 545. Also see http://fusion.gat.com/theory/Gyro for the most recent documentation.
[7] LUCE, T., *et al.*, Fusion Energy 2012 (Proc. 24th Int. Conf. San Diego, 2012) (Vienna: IAEA) CD-ROM file EX/P3-18.
[8] KINSEY, J.E., *et al.*, Nucl. Fusion **51** (2011) 083001.
[9] CANDY, J., *et al.*, Phys. Plasmas **16** (2009) 060704.
[10] SHIMADA, M., *et al.*, Nucl. Fusion **47** (2007) S1.
[11] MAGGI, C.F., *et al.* Nucl. Fusion **50**, 025023 (2010).
[12] MANTICA, P., *et al.*, Phys. Rev. Lett. **107** (2011) 135004.
[13] WALTZ, R.E., *et al.*, Phys. Plasmas **15** (2008) 014505.
[14] BELLI, E.A., *et al.*, Plasma Phys. Controlled Fusion **50** (2008) 095010.
[15] ITER Physics Expert Groups on Confinement and Transport and Confinement Modeling and Database, Nucl. Fusion **40** (2000) 1955.
[16] HOLLAND, C., *et al.*, accepted for publication in Nucl. Fusion (2012).
[17] WHITE, A.E., *et al.,* Phys. Plasmas **15** (2008) 056116.
[18] HOLLAND, C., *et al.*, Phys. Plasmas **16** (2009) 052301.
[19] RHODES, T.L., *et al.*, Nucl. Fusion **51** (2011) 063002.
[20] HOLLAND, C., *et al.*, Phys. Plasmas **18** (2011) 056113.
[21] McKEE, G.R., *et al.*, Rev. Sci. Instrum. **77** (2006) 10F104.
[22] DeBOO, J.C., *et al.*, Phys. Plasmas **19** (2012) 082518.
[23] HILLESHEIM, J.C., *et al.*, submitted to Phys. Rev. Lett. (2012).
[24] CANDY, J., Plasma Phys. Controlled Fusion **51** (2009) 105009.
[25] HOLLAND, C., *et al.*, Nucl. Fusion **52** (2012) 063028.